Recent advances in the plasma-assisted synthesis of silicon-based thin-films and nanostructures

On the coexistence of DAS and IMDD systems on the same fiber

1st Saverio Pellegrini
Politecnico di Torino
DET, Torino, Italy
saverio.pellegrini@polito.it

2nd Laura Hernandez-Martin
CSIC
Instituto de Optica, Madrid, Spain
laura.hernandez@io.cfmac.csic.es

3rd Ann M. Rosa Brusin
Politecnico di Torino
DET, Torino, Italy
ann.rosabrusin@polito.it

4th Giuseppe Rizzelli
Politecnico di Torino
Photonext Center, Torino, Italy
giuseppe.rizzelli@polito.it

5th Juan Diego Ania-Castañon
CSIC
Instituto de Optica, Madrid, Spain
jd.ania@csic.es

6th Gabriella Bosco
Politecnico di Torino
DET, Torino, Italy
gabriella.bosco@polito.it

7th Roberto Gaudino
Politecnico di Torino
DET, Torino, Italy
roberto.gaudino@polito.it

8th Hugo F. Martins
CSIC
Instituto de Optica, Madrid, Spain
hugo.martins@csic.es

***Abstract*—The paper experimentally addresses the new interesting topic of the coexistence of DAS signal and DWDM data signals on the same fibre. We demonstrate and characterize how high-peak-power DAS signals can generate significant impairments due to cross-talk arising from modulation instability. However, several solutions are readily demonstrated to significantly reduce the impact on the bit error ratio: employing frequency separations from the DAS channel and narrowband-filter at the data channel receiver, or counter-propagating signals. The work illustrates the key role that signal engineering plays in mitigating of coexistence-induced effects.**

***Index Terms*—DAS, chirped pulse, IMDD, coexistence, modulation instability**

I. Introduction

The dense installation of optical fibers for telecommunication purposes has laid the ground for coexistence with sensing techniques, exploiting the same infrastructure to detect hazards and anomalous mechanical vibrations occurring in the surroundings of fiber cables. Recent research has investigated the use of forward light state of polarization [1], [2] and phase [3] to detect anomalous events, demonstrating good reliability of both techniques with limited modification on the telecommunication system side. Conversely, exploiting external dedicated hardware, distributed acoustic sensing (DAS) based on phase-sensitive optical time-domain reflectometry (ϕOTDR) systems can detect and localize axial fiber strains with great sensitivity and accuracy, by sending high-power pulses into the fiber and processing the backscattered signal to retrieve strain and position information of events. Several works [4], [5] have demonstrated the effectiveness of DAS in characterizing natural and human-related activities and opening new scenarios for hazards early warnings. Without the use of highly complex architectures, including optical repeaters [6], DAS is typically limited to a few tens of km [7], making it suitable for coexistence with short-to-medium reach intensity modulated direct detection (IMDD) systems, which are today very common in metropolitan networks. Recently, the use of chirped pulse DAS (CP-ϕOTDR) technology [10], demonstrated high performances with simple operation, compared to standard ϕOTDR systems. Sending pulses with frequency modulation allows the use of direct detection whilst maintaining the linearity of the measurement [8]. Fig. 1a) shows a representation of the employed linearly chirped pulses (with starting frequency ν_0 at time τ_0, bandwidth $\Delta\nu$, and duration τ). A detuning $\delta\nu$ (corresponding to a perturbation ε) will be mapped into a time delay $\delta\tau$, which can be recovered by cross-correlation of subsequent backscattered traces.

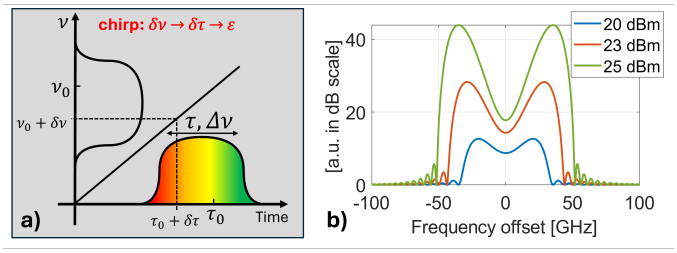

Fig. 1. a) Representation of the chirped pulse used for DAS [8]. b) Analytical MI spectral profile for different powers [9].

In this scenario, the required high-power DAS pulses propagating through the fiber can induce significant non-linear Kerr effects, such as modulation instability (MI). MI has been reported as the first non-linear effect to arise in DAS, limiting the pulse peak power to ∼23 dBm for long fibers, in conventional systems [11]. In Fig. 1b), we show the well-

This work was partially supported by SURENET project – funded by European Union – Next Generation EU within the PRIN 2022 program (D.D. 104 - 02/02/2022 Ministero dell'Università e della Ricerca). This manuscript reflects only the authors' views and opinions and the Ministry cannot be considered responsible for them.
We acknowledge financial support from the Spanish Ministry of Science and Innovation under grants PID2021-128000OB C21 and PRE2022-104176 and from the MCIN/AEI/10.13039/501100011033 and European Union "NextGenerationEU"/PRTR under grants RYC2021-035009-I, CNS2022-135925, CPP2022-009772.
This work was partially supported by the European Union - Next Generation EU under the Italian National Recovery and Resilience Plan (NRRP), Mission 4, Component 2, Investment 1.3, CUP E13C22001870001, partnership on "Telecommunications of the Future" (PE00000001 - program "RESTART").

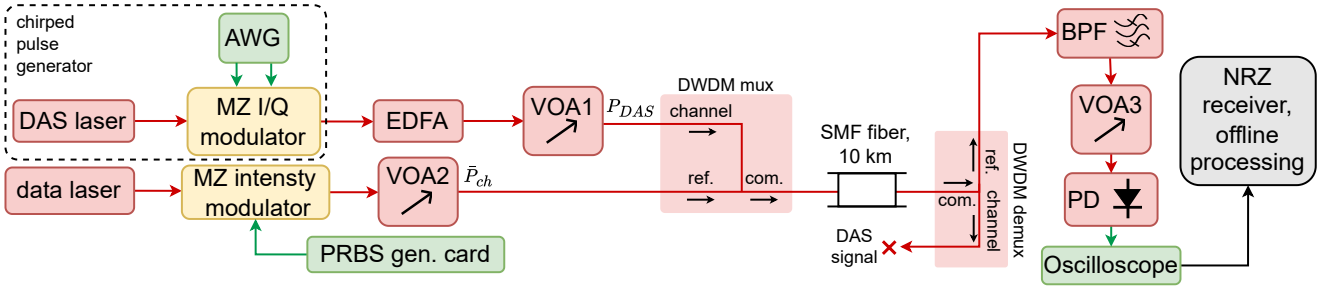

Fig. 2. Experimental setup scheme.

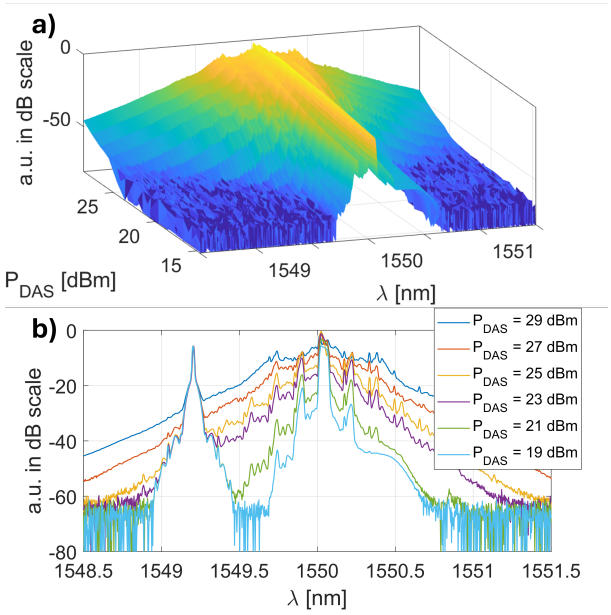

Fig. 3. MI-generated spectra with a) no co-propagating data channel versus P_{DAS} and wavelength and b) co-propagating data channel with Δf = 100 GHz spacing, for different P_{DAS} values. Note that the ratios of the average powers here depicted, do not reflect the ratios of the peak powers data/DAS (since data channel and DAS pulse had 50% and 2.4% duty cycles, respectively).

known analytic MI gain frequency response for 20 dBm, 23 dBm, and 25 dBm peak powers [9], [12], plotted as a function of the frequency offset from the pulse carrier. In particular, the angular frequency Ω_{max} at which the maximum MI gain is achieved is given by $\Omega_{max} = \pm\left(\frac{2\gamma P_0}{|\beta_2|}\right)^{1/2}$, being P_0 the pulse peak power, γ the fiber non-linear coefficient, and β_2 the group velocity dispersion constants [12]. In Fig. 1b), γ = 1.8 W^{-1}/km and β_2 = -22 ps^2/km. A co-propagating data channel, particularly in the surroundings of Ω_{max}, could then be strongly affected by the MI-induced crosstalk, with different consequences on the BER depending on the frequency separation and receiver optical filter bandwidth.

II. Experimental Setup

The experimental setup is reported in Fig. 2. A 100 Hz linewidth laser, centered at 1550 nm, followed by a Mach-Zehnder (MZ) I/Q modulator, driven by a 20 GS/s arbitrary waveform generator (AWG), generated the DAS pulses. The telecommunication side uses a standard setup based on a distributed-feedback (DFB) laser followed by a MZ intensity modulator. The electrical data stream signal is generated by a pseudo-random bit sequence (PRBS) card, at 10 Gbps with 2^{15}-1 bits periodicity. Four different central wavelengths were tested for the data channel: 1546.80 nm, 1548.40 nm, 1549.20 nm, and 1549.60 nm, corresponding to frequency spacings Δf from the DAS channel equal to 400 GHz, 200 GHz, 100 GHz, and 50 GHz, respectively. As shown in Fig. 2, the data channel is sent to the "ref." branch of the DWDM mux, with average power $\overline{P}_{ch}$ fixed at around -2 dBm. The DAS signal is sent once for each PRBS period (thus once every $\sim$3.2 μs, with 2.4% duty cycle), on the central part of the sequence. The repetition period is much smaller than the usual ones used for sensing (usually on the ms order). Nevertheless, since the practical importance of this study is placed mostly on the telecom side, we decreased it for practical reasons (namely, increasing the overlap between DAS pulse and telecom data). The pulse was shaped as a 4th-order Super-Gaussian envelope, with full-width-half-maximum (FWHM) duration τ = 80 ns and less than 10 ns of rise/fall edges, modulated between ν_0 = -1 GHz and -6 GHz with respect to the carrier frequency (total bandwidth $\Delta\nu$ = 5 GHz). Note that the electrical signal generated by the AWG has been equalized (pre-distorted to compensate for the hardware frequency-dependent losses + EDFA), reaching an optical pulse power variation across the entire chirp bandwidth which was below our measurement capabilities, i.e., less than 1 dB difference from ν_0 to $\nu_0 + \Delta\nu$. Right after the MZ I/Q block, an Erbium-Doped Fiber Amplifier (EDFA) amplifies the DAS pulse. To set its peak power P_{DAS}, one of the key parameters in our study, the variable optical attenuator 1 (VOA1, see Fig. 2) is opened/closed. The DAS pulse is sent to the "channel" branch of the DWDM mux (see Fig. 2), and both signals are merged ("com." branch in Fig. 2) and sent into a 10 km long SMF fiber. After fiber propagation, a DWDM demux is used to separate the channels and discard the DAS pulse, to focus on the co-propagation effect on data. The resulting signal is then passed through a bandpass optical filter (BPF) centered around the telecommunication channel, resulting in a rejection ratio of more than 60 dB for the DAS signal. The attenuator VOA3 adjusted the optical power to the dynamic range of the photodiode (PD), which electrically connects to the oscilloscope. For each of the four frequency spacings Δf,

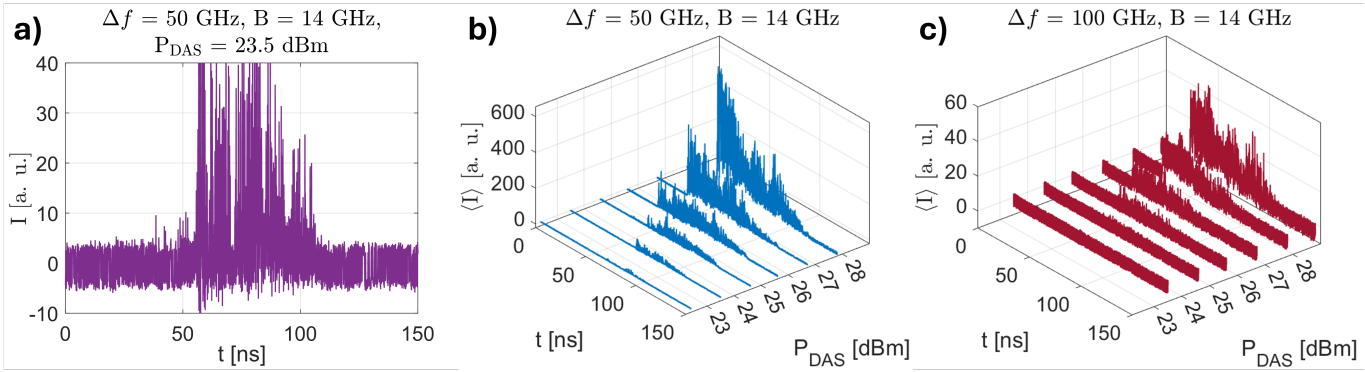

Fig. 4. Chirped pulse effect on the data channel when co-propagating for a) a single, non-averaged, trace with Δf = 50 GHz, B = 14 GHz, P_{DAS} = 23.5 dBm. 50-traces-average for each P_{DAS} is reported for b) Δf = 50 GHz, B = 14 GHz, and c) Δf = 100 GHz, B = 14 GHz. Different scales on the z-axis are intentionally used.

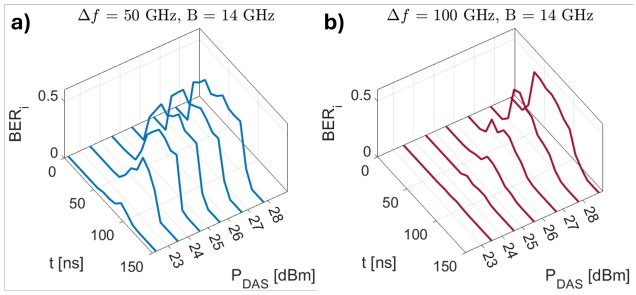

Fig. 5. Instantaneous BER computed along the pulse occurrence for a) Δf = 50 GHz, B = 14 GHz and b) Δf = 100 GHz, B = 14 GHz.

four values have been tested for the -3 dB bandwidth B of the optical BPF: 50 GHz, 30 GHz, 20 GHz, and 14 GHz, to address the different consequences on the data channel when including (or excluding) more MI-generated crosstalk. The received optical power when the DAS pulse is off, right before the PD, was set to -20 dBm, corresponding to a BER around $BER_{noDAS} = 10^{-4}$, computed offline for a Non-Return-to-Zero (NRZ) and B = 50 GHz.

III. Experimental Results and Discussion

To comprehensively illustrate the scenario of coexistence between DAS and telecom channels, Fig. 3a) shows the experimentally recorded average spectrum after propagation of the DAS pulse alone. The z-axis has arbitrary units (a.u.), in dB scale, normalized to the overall maximum value of the spectra. As previously discussed, the MI-generated crosstalk is strongly dependent on the pulse peak power, which finds experimental confirmation in Fig. 3a), as the spectrum broaden for increasing P_{DAS}. Fig 3b) shows a few overlapped spectra at different increasing pulse peak powers, coexisting with the data channel spaced at 100 GHz. There, the impact of the crosstalk induced by the MI on the data channel is clear, in particular for $P_{DAS} > 23$ dBm.

Before addressing the effect that the DAS pulse has on the data channel in terms of BER, we discuss its physical effect on the received NRZ signal. Fig. 4a) shows, for Δf = 50 GHz, B = 14 GHz, and P_{DAS} = 23.5 dBm, an isolated portion of the data stream represented by its intensity I, taken from the oscilloscope, right after the PD (the DC value was removed). The zoom is over a 150 ns time window that includes the 80 ns of DAS pulse co-propagation, where the effect of MI crosstalk is strong. Unaffected data stream is visible before ∼50 ns and after ∼100 ns, with 10 a.u. of modulation amplitude. To evaluate the dependency on Δf, B, and P_{DAS}, 50 traces like the one in Fig. 4a) have been recorded, and the average intensity evolution $\langle I \rangle$ versus time and P_{DAS} is reported in Figs. 4b-c). Here, the dependency of Ω_{max} with power is clear and expected (as discussed in Sec. I). Consequently, for the 50 GHz case, with increasing pulse peak powers, the MI crosstalk causes a huge distortion on the received data stream, with a power 60 times higher than the one of the data modulation amplitude (set by reference at 10 a.u.). Consistently, the effect is one order of magnitude weaker for the same condition in the 100 GHz case. Note also that for both frequency spacings, for a fixed P_{DAS}, as the chirped pulse frequency changes inside τ, the power transfer changes as well. This is very clear, in particular for P_{DAS} = 26 dBm to 29 dBm, in both Figs. 4b-c). The asymmetry can be explained because we are considering a $\Delta\nu = 5$ GHz "slice" of the MI curve (see Fig. 3a-b)), instead of just a single point, leading to some imbalance in the power transfer to the data. Another important consequence is the errors generation on the data channel, which could have a strong dependency on the bit position inside the pulse. This effect is shown in Fig. 5, where the instantaneous bit error rate (BER_i) is reported versus time and P_{DAS}. This parameter has been computed by counting the number of errors over 50 repetitions, considering slices of 100 bits (10 ns). For the smallest frequency separation, illustrated in Fig. 5a), the number of errors saturates around 0.5 at 26 dBm, meaning that every bit affected by the pulse is wrong (i.e., all bits are measured as "1"). With the same power level, the 100 GHz case, in Fig. 5b), is much less critical. Because of the weaker distortion, the imbalance of the BER inside the pulse is visible, particularly between 27 dBm and 29 dBm, as a consequence of the described MI crosstalk dependency on the pulse frequency detuning.

To compare performances with different Δf and B, the total BER is reported in Fig. 6 versus P_{DAS}. Each point has

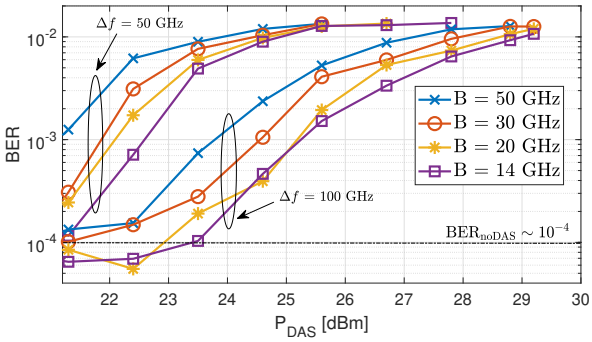

Fig. 6. BER curves versus P_{DAS} in different filtering and frequency separation conditions.

been computed by considering 200 μs of data, corresponding to ∼60 PRBS periods and the same number of DAS pulses. Two key insights can be drawn from the curves shown in Fig. 6. First, fixing Δf, narrowing the filter is fundamental to enhance the telecom channel performances, as it intuitively reduces the amount of MI-induced crosstalk (see Fig. 3b)). For Δf = 100 GHz in the range between 23 dBm to 27 dBm, before curve saturation, doubling B (from 14 GHz to 30 GHz, respectively purple and orange curves in Fig. 6) corresponds to roughly doubling the related BERs. Meanwhile, employing a Δf = 50 GHz, for equal BER values, the related DAS peak power is 2-3 dB lower. Notice how all curves saturate around 10^{-2}, further confirming that all bits affected by MI-induced crosstalk (see Fig. 5) are erroneous at high power levels, with all bits being detected as "1" during the DAS pulse overlap. Further tests have been carried out with larger spacings, 200 GHz and 400 GHz (same experimental setup as Fig. 2), and also counter-propagating DAS and data signals. Table I summarizes the main operational conditions that allow for the coexistence of the two systems when using B = 14 GHz. Particularly, P_{th} indicates the P_{DAS} threshold value where co-propagation starts to have consequences on the data channel. P_{sat} shows instead the power at which all the bits affected by co-propagation are considered wrong (i.e., in our case corresponding to a BER around 10^{-2}). As can be seen from Fig. 6 for 50 GHz and 100 GHz, P_{th} can be considered to be ∼22 dBm and ∼24 dBm, respectively. Lower powers do not appear to have any significant impact on the data channel. With Δf = 200 GHz, consequences on the BER start to appear at high values of P_{DAS}, which are hardly reached for practical DAS implementations. Δf = 400 GHz does not lead to consequences on the BER, for any considered scenario. As also experimentally demonstrated in [13], a counter-propagating DAS signal does not affect the data channel for any tested value of Δf and B.

IV. Conclusions

We have investigated the coexistence of CP-ϕOTDR systems with IMDD telecom data channels. Our results show the impact of MI crosstalk in terms of data distortion and instantaneous bit error rate (BER_i) during the co-propagation

TABLE I
CONSEQUENCES ON THE DATA CHANNEL FOR CO-/COUNTER-PROPAGATING SIGNALS, CONSIDERING B = 14 GHZ.

technique	Δf	P_{th}	P_{sat}
co-prop.	50 GHz	∼22 dBm	∼25 dBm
	100 GHz	∼24 dBm	∼28 dBm
	200 GHz	∼28 dBm	> 28 dBm
	400 GHz	-	-
counter-prop.	No cons. on the data channel.		

of DAS pulses. Additionally, we analyzed the total BER as a function of P_{DAS}, Δf and filter bandwidth B. At typical DAS launch powers around ∼23 dBm, coexistence with 100, 200, 400 GHz spaced channels results in negligible or no degradation of the data signal. However, a 50 GHz channel spacing is more critical, requiring the DAS peak power to be limited to $P_{DAS} \leq 21$ dBm when employing a narrowband filter.

References

[1] S. Pellegrini, L. Minelli, L. Andrenacci, G. Rizzelli, D. Pilori, G. Bosco, L. D. Chiesa, C. Crognale, S. Piciaccia, and R. Gaudino, "Overview on the state of polarization sensing: application scenarios and anomaly detection algorithms," *J. Opt. Commun. Netw.*, vol. 17, pp. A196–A209, 02 2025.

[2] C. J. Carver and X. Zhou, "Polarization sensing of network health and seismic activity over a live terrestrial fiber-optic cable," *Communications Engineering*, vol. 3, pp. 788–795, 07 2024.

[3] L. Andrenacci, D. Pilori, S. Pellegrini, L. Minelli, G. Bosco, C. Crognale, S. Piciaccia, and R. Gaudino, "Comparison between Phase and Polarization Sensing using Coherent Transceivers over Deployed Metro Fibers," in *Optical Fiber Communication Conference (OFC) 2024*, p. M2K.2, Optica Publishing Group, 2024.

[4] E. F. Williams, M. R. Fernández-Ruiz, R. Magalhaes, R. Vanthillo, Z. Zhan, M. González-Herráez, and H. F. Martins, "Distributed sensing of microseisms and teleseisms with submarine dark fibers," *Nature Communications*, vol. 10, 2019.

[5] J. Liu, S. Yuan, Y. Dong, B. Biondi, and H. Y. Noh, "TelecomTM: A Fine-Grained and Ubiquitous Traffic Monitoring System Using Pre-Existing Telecommunication Fiber-Optic Cables as Sensors," *Proc. ACM Interact. Mob. Wearable Ubiquitous Technol.*, vol. 7, 06 2023.

[6] E. Ip, Y.-K. Huang, M.-F. Huang, F. Yaman, G. Wellbrock, T. Xia, T. Wang, K. Asahi, and Y. Aono, "DAS Over 1,007-km Hybrid Link With 10-Tb/s DP-16QAM Co-Propagation Using Frequency-Diverse Chirped Pulses," *J. Lightw. Technol.*, vol. 41, pp. 1077–1086, 2023.

[7] M. R. Fernández-Ruiz, L. Costa, and H. F. Martins, "Distributed Acoustic Sensing Using Chirped-Pulse Phase-Sensitive OTDR Technology," *Sensors*, vol. 19, no. 20, 2019.

[8] L. Costa, H. F. Martins, S. Martín-López, M. R. Fernández-Ruiz, and M. González-Herráez, "Fully Distributed Optical Fiber Strain Sensor With 10^{-12} $\varepsilon/\sqrt{\text{Hz}}$ Sensitivity," *Journal of Lightwave Technology*, vol. 37, no. 18, pp. 4487–4495, 2019.

[9] M. Alem, M. A. Soto, and L. Thévenaz, "Analytical model and experimental verification of the critical power for modulation instability in optical fibers," *Opt. Express*, vol. 23, pp. 29514–29532, 11 2015.

[10] J. Pastor-Graells, H. F. Martins, A. Garcia-Ruiz, S. Martin-Lopez, and M. Gonzalez-Herraez, "Single-shot distributed temperature and strain tracking using direct detection phase-sensitive OTDR with chirped pulses," *Opt. Express*, vol. 24, pp. 13121–13133, 06 2016.

[11] H. F. Martins, S. Martin-Lopez, P. Corredera, P. Salgado, O. F. ao, and M. González-Herráez, "Modulation instability-induced fading in phase-sensitive optical time-domain reflectometry," *Opt. Lett.*, vol. 38, pp. 872–874, 03 2013.

[12] G. P. Agrawal, "Chapter 5 - optical solitons," in *Nonlinear Fiber Optics (Fifth Edition)* (G. Agrawal, ed.), Optics and Photonics, pp. 129–191, Boston: Academic Press, fifth edition ed., 2013.

[13] Z. Jia, L. A. Campos, M. Xu, H. Zhang, M. Gonzalez-Herraez, H. F. Martins, and Z. Zhan, "Experimental Coexistence Investigation of Distributed Acoustic Sensing and Coherent Communication Systems," in *Optical Fiber Communications Conf. and Exhibition (OFC)*, 2021.